Enhancement of spin-mixing conductance by *s-d* orbital hybridization in heavy metals

Adam B. Cahaya,[1,*] Rico M. Sitorus,[1] Anugrah Azhar,[2] Ahmad R. T. Nugraha,[3] and Muhammad Aziz Majidi[1]

[1]*Department of Physics, Faculty of Mathematics and Natural Sciences, Universitas Indonesia, Depok 16424, Indonesia*

[2]*Physics Study Program, Faculty of Sciences and Technology, Syarif Hidayatullah State Islamic University Jakarta, South Tangerang 15412, Indonesia*

[3]*Research Center for Quantum Physics, National Research and Innovation Agency (BRIN), South Tangerang 15314, Indonesia*

(Received 12 January 2022; revised 13 June 2022; accepted 22 June 2022; published 29 June 2022)

In a magnetic multilayer, the spin transfer between localized magnetization dynamics and itinerant conduction spin arises from the interaction between a normal metal and an adjacent ferromagnetic layer. The spin-mixing conductance then governs the spin-transfer torques and spin pumping at the magnetic interface. Theoretical description of spin-mixing conductance at the magnetic interface often employs a single conduction-band model. However, there is orbital hybridization between conduction *s* electron and localized *d* electron of the heavy transition metal, in which the single conduction-band model is insufficient to describe the *s-d* orbital hybridization. In this work, using the generalized Anderson model, we estimate the spin-mixing conductance that arises from the *s-d* orbital hybridization. We find that the orbital hybridization increases the magnitude of the spin-mixing conductance.

DOI: 10.1103/PhysRevB.105.214438

I. INTRODUCTION

The technological potential of magnetic devices based on transition metals for spin-current manipulation has pushed research forward in the spintronics area [1]. The basic structure of a magnetic device is a magnetic multilayer. In spin-based memory systems, the interaction between normal metal and ferromagnetic metal can cause the magnetization direction to change [2].

In a magnetic multilayer, magnetization dynamics can be induced by spin current via the spin-transfer torque effect [3]. When the nonmagnetic layer has a finite spin accumulation $\boldsymbol{\mu}$, which represents the difference of the spin-dependent electrochemical potential, the magnetization near the ferromagnetic interface experiences a torque $\boldsymbol{\tau}$ due to spin transfer [4]:

$$\boldsymbol{\tau} = g_{\uparrow\downarrow}\mathbf{m} \times (\mathbf{m} \times \boldsymbol{\mu}), \tag{1}$$

where $g_{\uparrow\downarrow}$ is the spin-mixing conductance. Reciprocally, in spin pumping, the spin current can be induced by magnetization dynamic $\mathbf{m}$ via the exchange interaction between magnetization and spin of the conduction electron [5]. An adiabatic precession of the magnetization pumps a spin current from the ferromagnet to the nonmagnetic layer with a polarization [6–8] of

$$\mathbf{J} = g_{\uparrow\downarrow}\mathbf{m} \times \dot{\mathbf{m}}. \tag{2}$$

Both spin-transfer torque and spin-pumping effects are governed by the same $g_{\uparrow\downarrow}$, which has a complex value with a comparably small imaginary term [9].

Spin-mixing conductance was originally described using spin-dependent scattering theory [5]. The basic theoretical models of spin-mixing conductance utilizes a noninteracting electron model for the nonmagnetic metal [10,11]. While this is certainly appropriate for free-electron-like metals, it is less so for heavy transition metals [12]. To accommodate the localized symmetry of the *d* electron, a linear response theory description of spin-mixing conductance has been developed [11]. However, there are few theoretical studies exploring the spin-mixing conductance of heavy metals with the interacting electron model [13]. Therefore, a better understanding of the spin-mixing conductance of heavy metals is required.

The theoretical description of spin-mixing conductance is often simplified in order to focus on a certain aspect or interaction that dominates a particular setup [14]. In the spin-pumping setup involving a heavy-metal system discussed in this article, we focus on the effect of electron-electron interaction at the nonmagnetic heavy-metal layer. While the effect of electron interaction on spin-mixing conductance has been studied using the Stoner model and phenomenological Hubbard parameter U [15–17], a more realistic model of the heavy-metal system requires orbital hybridization [18], for example, the Anderson model [19]. In the Anderson model, a *d* electron is treated as an impurity, with well-localized energy dispersion [20]. For describing a heavy metal, however, we need to consider a *d* electron with a more generalized dispersion [21]. This article aims to theoretically estimate the electron-electron interaction correction factor due to the *s-d* orbital hybridization of a heavy metal as illustrated in Fig. 1.

In this article, we first analyze the linear response theory of spin density in a heavy transition metal using the Anderson model in Sec. II. In Sec. III, we show that the orbital hybridization enhances $g_{\uparrow\downarrow}$ of the interface of ferromagnet and heavy transition metal (Ta, W, Ir, Pt, or Au). Lastly, we summarize our findings in Sec. IV.

*adam@sci.ui.ac.id

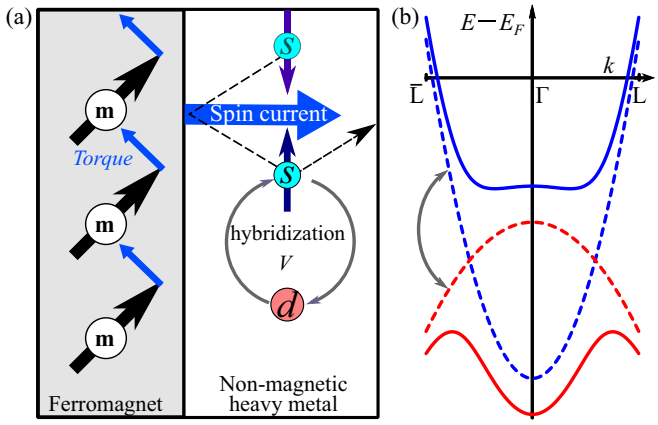

FIG. 1. (a) The interface of magnetic and heavy metals can be modeled as a ferromagnetic layer with localized magnetic moments and itinerant conduction electrons. The interaction of magnetic moments and conduction spin induces spin-transfer torque and spin current pumping in ferromagnetic layer and nonmagnetic layer, respectively. (b) In heavy metal, there is orbital hybridization between conduction s electron and d electron [19] with parabolic dispersions [21].

II. LINEAR RESPONSE THEORY IN HEAVY TRANSITION METAL

Near the magnetic interface, the exchange interaction between the localized magnetic moments $\mathbf{m}$ at the magnetic interface and the conduction spin $\boldsymbol{\sigma}$ can be written in the following Hamiltonian,

$$H_{\rm ex} = -J \int d\mathbf{r}\delta(\mathbf{r})\mathbf{m}\cdot\boldsymbol{\sigma}(\mathbf{r}), \tag{3}$$

where the exchange constant in the strong screening limit is $J = M_s/(\gamma\mathcal{N}_F)$ [4,11]. M_s and γ are saturation magnetization and gyromagnetic ratio of the ferromagnetic insulator, respectively. $\mathcal{N}_F$ is the density of states of the conduction electron at the Fermi level.

Using linear response theory, one can show the response of $\boldsymbol{\sigma}$ to $\mathbf{m}$ via spin susceptibility χ_{ij},

$$\sigma_i(\mathbf{r},t) = J\int d\mathbf{r}'dt'\chi_{ij}(\mathbf{r}-\mathbf{r}',t-t')m_j(t')\delta(\mathbf{r}'), \tag{4}$$

where

$$\chi_{ij}(\mathbf{r},t) = \frac{i}{\hbar}\Theta(t)\langle[\sigma_i(\mathbf{r},t),\sigma_j(\mathbf{0},0)]\rangle. \tag{5}$$

Here $\Theta(t)$ is the Heaviside step function. In an isotropic medium, $\chi_{ij} = \delta_{ij}\chi$ can be written in terms of χ^{-+} and χ^{+-}:

$$\chi = \chi^{-+} + \chi^{+-}, \tag{6}$$

where

$$\chi^{-+}(\mathbf{r},t) = \frac{i}{\hbar}\Theta(t)\langle[\sigma^-(\mathbf{r},t),\sigma^+(\mathbf{0},0)]\rangle,$$
$$\chi^{+-}(\mathbf{r},t) = \frac{i}{\hbar}\Theta(t)\langle[\sigma^+(\mathbf{r},t),\sigma^-(\mathbf{0},0)]\rangle.$$

Here $\sigma_\pm = (\sigma_x \pm i\sigma_y)/2$ and σ_a $(a = x, y, z)$ are Pauli matrices. Since χ^{+-} can be obtained by replacing $+$ and $-$, it is convenient to discuss χ^{-+}.

For a noninteracting simple metal with parabolic dispersion $E_{\mathbf{k}} = E_0 + \hbar^2k^2/2m^*$, χ in a small-ω limit is [11]

$$\begin{aligned}\lim_{\omega\to0}\chi_0(\mathbf{q},\omega) &= \lim_{\omega\to0}\sum_{\mathbf{k}}\frac{f_{\mathbf{k}}-f_{\mathbf{k}+\mathbf{q}}}{E_{\mathbf{k}+\mathbf{q}}-E_{\mathbf{k}}+\hbar\omega+i0^+}\\ &= \frac{mk_F}{\pi^2\hbar^3}\left(\frac{1}{2}+\frac{k_F^2-\left(\frac{q}{2}\right)^2}{2k_Fq}\ln\left|\frac{1+\frac{q}{2k_F}}{1-\frac{q}{2k_F}}\right|\right)\\ &\quad + i\omega\frac{m^2\Theta(2k_F-q)}{2\pi\hbar^3q}\\ &\equiv \chi_0^r(q) + i\omega\chi_0^i(q),\end{aligned} \tag{7}$$

where $f_{\mathbf{k}}$ is the low-temperature Fermi-Dirac distribution with wave vector $\mathbf{k}$.

This single-band picture is appropriate for simple metals, such as light transition metals. Meanwhile, for heavy transition metal such as Au, W, Ta, and Pt, a localized $5d$-electron can mixed with the $6s$ band, as illustrated in the band structure [see Fig. 1(b)]. The band structure can be obtained from density functional theory (DFT) software [22,23] (see the Appendix). Because of that, to determine the $g_{\uparrow\downarrow}$ of heavy metal, we need to modify the single-band Hamiltonian with an appropriate Hamiltonian that accommodates the hybridization of s and d electrons.

In the second quantization, the interactions in a heavy-metal system near the interface that is illustrated in Fig. 1 can be written with the following Hamiltonian based on the Anderson model [19,20]:

$$H_0 = \sum_{\mathbf{k}\alpha}\begin{pmatrix}a^\dagger_{\mathbf{k}\alpha} & b^\dagger_{\mathbf{k}\alpha}\end{pmatrix}\begin{pmatrix}E^s_{\mathbf{k}} & V\\ V & E^d_{\mathbf{k}}\end{pmatrix}\begin{pmatrix}a_{\mathbf{k}\alpha}\\ b_{\mathbf{k}\alpha}\end{pmatrix}, \tag{8}$$

where V is the hybridization parameter, $a^\dagger_{\mathbf{k}\alpha}(a_{\mathbf{k}\alpha})$ is the creation (annihilation) operator of the s electron with wave vector $\mathbf{k}$ and spin α and $b^\dagger_{j\alpha}(b_{j\alpha})$ is the creation (annihilation) operator of the d electron with spin α. The second term corresponds to the s-d hybridization. Here $\boldsymbol{\sigma}_{\alpha\beta}$ are the Pauli vectors. The energy dispersion of s and d electrons can be assumed to be parabolic,

$$E^{s,d}_{\mathbf{k}} = E^{s,d}_0 + \frac{\hbar^2k^2}{2m^*_{s,d}}, \tag{9}$$

as illustrated in Fig. 4.

As illustrated in Fig. 1, the s electron dominates the spin-mixing process at the interface. Therefore, we can define $\boldsymbol{\sigma}(\mathbf{r})$ from the spin density of the s electron

$$\boldsymbol{\sigma}(\mathbf{r}) = \sum_{\mathbf{kq}\alpha\beta}e^{i\mathbf{q}\cdot\mathbf{r}}\boldsymbol{\sigma}_{\alpha\beta}a^\dagger_{\mathbf{k}+\mathbf{q}\alpha}a_{\mathbf{k}\beta}. \tag{10}$$

The susceptibility and its Fourier transform $\chi(\omega) = \int dt e^{i\omega t}\chi(t)$ can be determined by evaluating its time derivation using the Heisenberg equation

$$\frac{\partial F(t)}{\partial t} = \frac{1}{i\hbar}[F(t),H_0] \;\leftrightarrow\; \hbar\omega F(\omega) = [F(\omega),H_0]. \tag{11}$$

TABLE I. Parameters of conduction electrons and its hybridization. The values are obtained using fitting from DFT [22–24] (see the Appendix).

Heavy metal	Crystal				Without spin-orbit coupling				With spin-orbit coupling			
element	structure	a (Å)	Path	Band	V (eV)	$E_0^{s,d}$ (eV)	$m^*_{s,d}/m_e$	$U_{sd}\mathcal{N}_F^s$	V (eV)	$E_0^{s,d}$ (eV)	$m^*_{s,d}/m_e$	$U_{sd}\mathcal{N}_F^s$
Au	fcc	2.88	$\Gamma-\mathrm{L}$	s	2.44	−8.86	1.19	0.09	2.53	−8.23	1.28	0.15
				d		−4.27	−4.19			−4.05	−5.46	
W	bcc	2.74	$\Gamma-\mathrm{N}$	s	2.38	−8.74	0.84	0.10	2.34	−8.58	0.86	0.11
				d		−1.98	−2.01			−2.09	−2.17	
Ta	bcc	2.87	$\Gamma-\mathrm{N}$	s	2.28	−7.18	0.78	0.22	2.25	−7.02	0.79	0.25
				d		0.12	−1.56			−0.02	−1.70	
Ir	fcc	2.74	$\Gamma-\mathrm{L}$	s	3.76	−8.95	0.97	0.27	3.62	−9.08	1.12	0.27
				d		−2.94	−2.96			−2.67	−3.33	
Pt	fcc	2.77	$\Gamma-\mathrm{L}$	s	3.22	−8.58	1.21	0.30	3.32	−8.17	1.12	0.37
				d		−3.14	−5.07			−3.03	−5.01	

Here H_0 is the unperturbed Hamiltonian in Eq. (8). Due to the hybridization of s and d orbitals, combinations of creation $(a^\dagger, b^\dagger)$ and annihilation (a, b) operators appear when the commutations are evaluated. For convenience, we define

$$\chi^{-+}_{abcd}(\mathbf{q},t)=\sum_{\mathbf{k}}\chi^{-+}_{abcd}(\mathbf{k},\mathbf{q},t), \tag{12}$$

where

$$\chi^{-+}_{abcd}(\mathbf{k},\mathbf{q},t)=\frac{i}{\hbar}\Theta(t)\sum_{\mathbf{k}'\mathbf{q}'}\langle[a_{\mathbf{k}+\mathbf{q}\downarrow}(t)b_{\mathbf{k}\uparrow}(t),c_{\mathbf{q}'\uparrow}(0)d_{\mathbf{k}'\downarrow}(0)]\rangle. \tag{13}$$

χ_{aaaa} in the frequency domain can now be obtained from a matrix relation

$$\begin{pmatrix} E^s_{\mathbf{k}+\mathbf{q}}-E^s_{\mathbf{k}}+\hbar\omega & -V & 0 & V \\ V & E^s_{\mathbf{k}+\mathbf{q}}-E^d_{\mathbf{k}}+\hbar\omega & -V & 0 \\ 0 & V & E^d_{\mathbf{k}+\mathbf{q}}-E^s_{\mathbf{k}}+\hbar\omega & -V \\ -V & 0 & V & E^d_{\mathbf{k}+\mathbf{q}}-E^d_{\mathbf{k}}+\hbar\omega \end{pmatrix}\begin{pmatrix}\chi_{aaaa}\\ \chi_{abaa}\\ \chi_{baaa}\\ \chi_{bbaa}\end{pmatrix}=\begin{pmatrix} f^s_{\mathbf{k}}-f^s_{\mathbf{k}+\mathbf{q}}\\ 0\\ 0\\ 0\end{pmatrix}. \tag{14}$$

Let us note that since susceptibility is a retarded response [8], ω has a negligibly small imaginary term $\omega=\lim_{\eta\to0}(\omega+i\eta)$ as in Eq. (7). By solving the linear equation, the leading term of V-dependent spin susceptibility of the conduction of the s electron χ_{aaaa} is

$$\chi_{aaaa}(\mathbf{k},\mathbf{q},\omega)\simeq\frac{\chi_0(\mathbf{k},\mathbf{q},\omega)}{1-U_{sd}(\mathbf{k},\mathbf{q})\chi_0(\mathbf{k},\mathbf{q},\omega)},$$

$$\chi_0(\mathbf{k},\mathbf{q},\omega)=\frac{f^s_{\mathbf{k}}-f^s_{\mathbf{k}+\mathbf{q}}}{E^s_{\mathbf{k}+\mathbf{q}}-E^s_{\mathbf{k}}+\hbar\omega+i0^+}. \tag{15}$$

Here U_{sd} is the electron-electron interaction parameter due to s-d hybridization,

$$U_{sd}(\mathbf{k},\mathbf{q})=\frac{\left(E^s_{\mathbf{k}+\mathbf{q}}+E^d_{\mathbf{k}+\mathbf{q}}-E^s_{\mathbf{k}}-E^d_{\mathbf{k}}\right)|V|^2}{\left(f^s_{\mathbf{k}}-f^s_{\mathbf{k}+\mathbf{q}}\right)\left(E^s_{\mathbf{k}+\mathbf{q}}-E^d_{\mathbf{k}}\right)\left(E^s_{\mathbf{k}}-E^d_{\mathbf{k}+\mathbf{q}}\right)}. \tag{16}$$

The hybridization parameter V can be obtained by fitting the band structure obtained from DFT using WANNIER90 software [24]. The values of the parameters are listed in Table I. Since the spin-orbit interaction in a heavy metal is large, we also evaluate the parameters.

Using the localization of $\partial f_{\mathbf{q}}/\partial E_{\mathbf{q}}\approx-\delta(E-E_F)$, one can show that

$$\lim_{q,\omega\to0}\chi(\mathbf{q},\omega)=\lim_{q\ll k}\sum_{\mathbf{k}}\chi^{-+}_{aaaa}(\mathbf{k},\mathbf{q},\omega\to0)$$

$$=\frac{\chi^r_0(0)}{1-U_{sd}\mathcal{N}_F^s}+\frac{i\omega\chi^i_0(q)}{\left(1-U_{sd}\mathcal{N}_F^s\right)^2}, \tag{17}$$

where χ^r_0 and χ^i_0 are defined in Eq. (7) and

$$U_{sd}\mathcal{N}_F^s=\lim_{q\ll k_F}\sum_{\mathbf{k}}U_{sd}(\mathbf{k},\mathbf{q})\chi_{aaaa}(\mathbf{k},\mathbf{q},0)$$

$$=\frac{(m^*_d+m^*_s)|V|^2}{m^*_d[E_s(k_F)-E_d(k_F)]^2} \tag{18}$$

characterizes the enhancement due to the orbital hybridization. This enhancement parameter is similar to the Stoner parameter $U\mathcal{N}_F$ that enhances the static magnetic susceptibility. Furthermore, for Au and W without spin-orbit interaction,

$$U_{sd}\mathcal{N}_F^s\approx U\mathcal{N}_F,$$

where U is the phenomenological Hubbard parameter [15] (see Table II). However, $U_{sd}(k_F,0)\mathcal{N}_F^s<U\mathcal{N}_F$ for Ta, Ir, and Pt. Table II also shows that the spin-orbit interaction of the heavy metals increases $U_{sd}\mathcal{N}_F^s$.

TABLE II. Spin-mixing conductance [25] and the enhancement factor due to orbital hybridization of 5*d* heavy transition metals (HM) (see Table I). The electron-electron interaction parameter due to *s*-*d* hybridization $U_{sd}\mathcal{N}_F^s$ (with and without SOI) is comparable to the Stoner parameter $U\mathcal{N}_F$ due to electron-phonon interaction [15].

HM (5*d*)	$U\mathcal{N}_F$ [15]	$U_{sd}\mathcal{N}_F^s$ (with SOI)	$g_{\uparrow\downarrow}(10^{18}\ \mathrm{m}^{-2})$ $Y_3Fe_5O_{12}$|HM [25]	$g_{\uparrow\downarrow}(10^{19}\ \mathrm{m}^{-2})$ Co|HM [28]
Au	0.050	0.09 (0.15)	2.7 ± 0.2	1.0 ± 0.1
W	0.102	0.10 (0.11)	4.5 ± 0.4	1.2 ± 0.1
Ta	0.335	0.22 (0.25)	5.4 ± 0.5	1.0 ± 0.1
Ir	0.290	0.27 (0.22)		2.4 ± 0.2
Pt	0.590	0.30 (0.37)	6.9 ± 0.6	6.0 ± 0.2

III. ENHANCEMENT OF SPIN-MIXING CONDUCTANCE

The spin current generation due to the exchange interaction between conduction spin and **m** can be determined from the spin angular momentum loss due to the relative direction between conduction spin **s** and **m** [7,8]:

$$\mathbf{J}(t) = J \int d^3\mathbf{r}\boldsymbol{\sigma}(\mathbf{r}, t) \times \mathbf{m}(\mathbf{r}, t). \tag{19}$$

Using the relation of χ and $\boldsymbol{\sigma}$, one can obtain the spin current from Eq. (19):

$$\begin{aligned}\mathbf{J}(t) &= J \int d^3\mathbf{r}\boldsymbol{\sigma}(\mathbf{r}, t) \times \mathbf{m}(\mathbf{r}, t) \\ &= \mathbf{m}(t) \times \dot{\mathbf{m}}(t) \lim_{\omega\to 0} J^2 \sum_{\mathbf{qk}} \frac{\partial \mathrm{Im}\chi_{aaaa}(\mathbf{k}, \mathbf{q}, \omega)}{\partial\omega}. \\ &\equiv g_{\uparrow\downarrow}\mathbf{m}(t) \times \dot{\mathbf{m}}(t).\end{aligned} \tag{20}$$

Therefore, the spin-mixing conductance is enhanced by the orbital hybridization

$$g_{\uparrow\downarrow} = \lim_{\omega\to 0} J^2 \sum_{\mathbf{qk}} \frac{\partial \mathrm{Im}\chi_{aaaa}(\mathbf{k}, \mathbf{q}, \omega)}{\partial\omega} = \frac{J^2 \sum_{\mathbf{q}} \chi_0^i(q)}{\left[1 - U_{sd}(k_F, 0)\mathcal{N}_F^s\right]^2}. \tag{21}$$

Therefore, the spin-mixing conductance is

$$g_{\uparrow\downarrow} = \frac{g_{\uparrow\downarrow}^0}{\left(1 - U_{sd}\mathcal{N}_F^s\right)^2}. \tag{22}$$

Here $U_{sd}\mathcal{N}_F^s$ is the effective electron-electron interaction parameter described in Eq. (18), and

$$g_{\uparrow\downarrow}^0 \simeq \frac{\pi}{8}\left(\frac{M_s}{\gamma}\right)^2 \tag{23}$$

is independent of the heavy metal [4].

Figure 2 shows the enhancement of spin-mixing conductance of an insulating ferromagnet $Y_3Fe_5O_{12}$ and a heavy metal (HM) as a function of $U_{sd}\mathcal{N}_F^s$. For $Y_3Fe_5O_{12}$ with the magnetic moment $M_{Y_3Fe_5O_{12}} = 3\mu_B$ and unit cell lattice constant $a_{Y_3Fe_5O_{12}} = 5.4$ Å [26,27], spin-mixing conductance per unit area $g_{\uparrow\downarrow}^0/A$ can be estimated to be

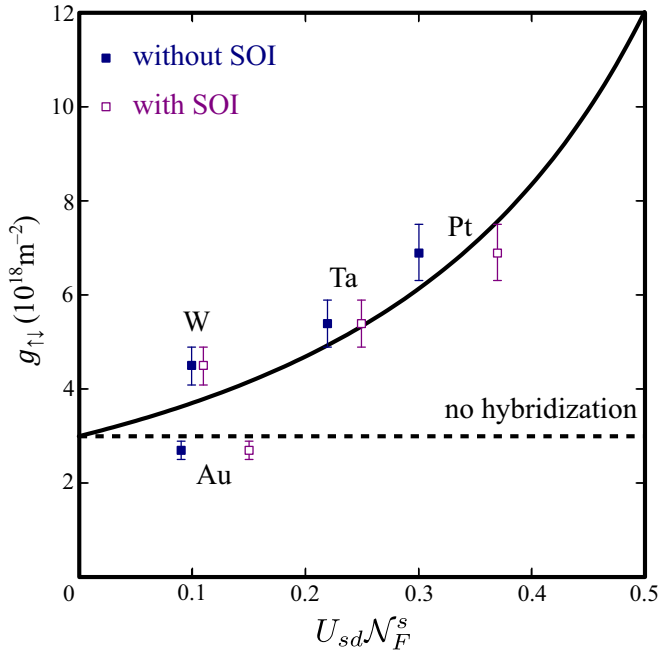

FIG. 2. Enhancement of spin-mixing conductance $g_{\uparrow\downarrow}$ of yttrium iron garnet ($Y_3Fe_5O_{12}$) and 5*d* heavy transition metal as a function $U_{sd}\mathcal{N}_F^s$, which characterizes the orbital hybridization. Filled square points are evaluated without spin-orbit interaction (SOI) while unfilled square points are values with SOI. Dashed and full lines are the values without and with hybridization, respectively. Here $g_{\uparrow\downarrow}^0(Y_3Fe_5O_{12}) = 3 \times 10^{18}\ \mathrm{m}^{-2}$. The experimental data of the interface of $Y_3Fe_5O_{12}$ and 5*d* transition metals are taken from Ref. [25], as summarized in Table II.

$$\frac{g_{\uparrow\downarrow}^0(Y_3Fe_5O_{12}|\mathrm{HM})}{A} = \frac{\pi(M_{Y_3Fe_5O_{12}}/\gamma_{Y_3Fe_5O_{12}})^2}{8a_{Y_3Fe_5O_{12}}^2} \approx 3 \times 10^{18}\ \mathrm{m}^{-2}. \tag{24}$$

The result is in agreement with the experimental work of Ref. [25]. This indicates that the *s*-*d* orbital hybridization induces an effective electron-electron interaction on the conduction *s* electron of the heavy transition metal and increases the spin-mixing conductance at its interface with a ferromagnetic insulator.

The discussion so far focuses on the case when the ferromagnetic layer is insulating. In an insulating magnetic interface, the orbital hybridization dominates the scattering for the interface of a ferromagnetic insulator and heavy metal, because only the heavy metal contributes to the conduction electrons. However, in the case of a metallic ferromagnet, the interactions of a conduction electron near the interface is more complicated. For a metallic ferromagnet (e.g., cobalt), to capture the complexity of the heavy-metal system [14], the enhancement factor should be replaced by a phenomenological parameter of the Stoner model [4,29],

$$g_{\uparrow\downarrow}(\mathrm{Co}|\mathrm{HM}) = \frac{g_{\uparrow\downarrow}^0(\mathrm{Co}|\mathrm{HM})}{(1 - U\mathcal{N}_F)^2}, \tag{25}$$

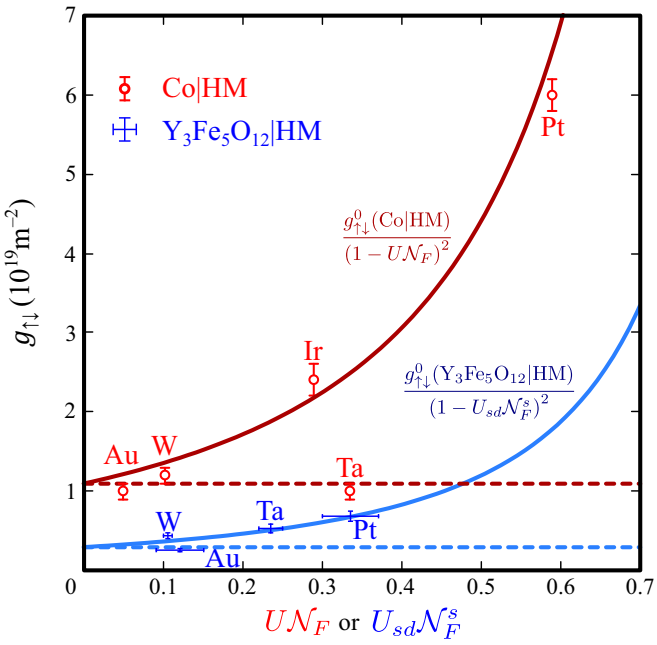

FIG. 3. Spin-mixing conductance $g_{\uparrow\downarrow}$ of (a) $Y_3Fe_5O_{12}$|heavy metal (HM) and (b) Co|HM. Dashed blue and red lines are the values without hybridization for $Y_3Fe_5O_{12}$ and Co, respectively. Full blue and red lines show the values with hybridization for $Y_3Fe_5O_{12}$ and Co, respectively. While $Y_3Fe_5O_{12}$ is an insulating ferromagnet, Co is a metallic ferromagnet. Experimental data of $Y_3Fe_5O_{12}$|HM and Co|HM are taken from Refs. [25,28], respectively (see Table II). For a metallic ferromagnet such as Co, the enhancement is characterized by the Stoner parameter $U\mathcal{N}_F$. On the other hand, for an insulating ferromagnet such as $Y_3Fe_5O_{12}$, the enhancement is dominated by *s*-*d* hybridization $U_{sd}\mathcal{N}_F^s$ (averaged from values in Fig. 2).

where

$$\frac{g^0_{\uparrow\downarrow}(\mathrm{Co|HM})}{A}=\frac{\pi d_{\mathrm{Co}}}{8V_{\mathrm{Co}}}\left(\frac{M_{\mathrm{Co}}}{\gamma_{\mathrm{Co}}}\right)^2\approx 1.1\times 10^{19}\mathrm{m}^{-2} \tag{26}$$

is the unenhanced spin-mixing conductance of the bilayer of HM and Co with width $d_{\mathrm{Co}}=10$ Å [28], magnetic moment $M_{\mathrm{Co}}=1.60\mu_B$, and cell volume $V_{\mathrm{Co}}=22$ Å^3 [26,30].

Figure 3 shows the agreement of Eq. (25) with the experiment of a metallic ferromagnet and Eq. (22) with the experiment of insulating ferromagnet. Co|HM has a larger $g_{\uparrow\downarrow}$ than $Y_3Fe_5O_{12}$ because the conduction spin can penetrate into a metallic ferromagnet and interact with more magnetic moments. When the ferromagnet layer is an insulator, the conduction electron purely originates from the heavy transition metal. Therefore, *s*-*d* hybridization dominates the electron-electron interaction and our model is more appropriate.

IV. CONCLUSIONS

To summarize, we discuss the effect of *s*-*d* orbital hybridization on the spin-mixing conductance of the interface of ferromagnet and heavy metal. Using a generalized Anderson model, we study the linear response theory of conduction spin near a magnetic interface. At the magnetic interface, the hybridization of the conduction *s* electron and localized *d* electron of a heavy transition metal increases the spin susceptibility of a heavy transition metal and subsequently enhances the spin-mixing conductance of the interface of ferromagnetic and 5*d* transition metals.

For a bilayer of a ferromagnetic metal and a heavy metal, the enhancement of spin-mixing conductance is characterized by an electron-electron interaction parameter in the Stoner model $U\mathcal{N}_F$, as illustrated in Fig. 3. Meanwhile, for a bilayer of a ferromagnetic insulator and a heavy metal, the enhancement is characterized by the electron-electron interaction parameter $U_{sd}\mathcal{N}_F^s$ due to orbital hybridization that depends on the hybridization energy V and the dispersion of *s* and *d* electrons. These parameters can be obtained by analyzing the band structure obtained from DFT. Figure 2 shows the agreement of our theory and the experimental values of the bilayer of $Y_3Fe_5O_{12}$ and 5*d* transition metal.

ACKNOWLEDGMENTS

We thank Universitas Indonesia for funding this research through PUTI Grant No. NKB-469/UN2. RST/HKP.05.00/2022.

APPENDIX: ENERGY DISPERSION AND DENSITY OF STATES OF 5*d* TRANSITION METALS

In this article, we analyze the orbital mixing of Ta, W, Ir, Pt, and Au. The orbital mixing occurs because of the hybridization between conduction (*s* band) and localized (*d* band, illustrated by DOS_d) electrons [21]. The hybridized energy bands due to Hamiltonian in Eq. (8) are

$$E_{12}(\mathbf{k})=\frac{E^s_{\mathbf{k}}+E^d_{\mathbf{k}}}{2}\pm\sqrt{\left(\frac{E^s_{\mathbf{k}}-E^d_{\mathbf{k}}}{2}\right)^2+|V|^2}. \tag{A1}$$

As illustrated in Fig. 4, the partially filled band near the Fermi surface is chosen as $E_1(k)$, while the band at the bottom of the density of states is chosen as $E_2(k)$. Ir, Pt, and Au have fcc structures. Figures 4(a) and 4(b) illustrate the band structure along $\mathrm{L}-\Gamma-\mathrm{X}$ symmetry points and density of states, respectively. On the other hand, Ta and W have bcc structures. Figures 4(c) and 4(d) illustrate the band structure along $\mathrm{N}-\Gamma-\mathrm{H}$ symmetry points and density of states, respectively.

By assuming $E^s_{\mathbf{k}}$ and $E^d_{\mathbf{k}}$ to be parabolic near Γ point, the band structure parameters can be obtained by fitting the band structure obtained from DFT. The sum of E_1 and E_2

$$E_1+E_2=E^s_{\mathbf{k}}+E^d_{\mathbf{k}}\equiv E^+_\Gamma+\frac{\hbar^2k^2}{2m^*_+} \tag{A2}$$

can be used to obtain

$$E^+_\Gamma=E^s_0+E^d_0,\quad \frac{1}{m^*_+}=\frac{1}{m^*_s}+\frac{1}{m^*_d}.$$

On the other hand, their difference

$$\begin{aligned}E_1-E_2&=\sqrt{\left(E^s_{\mathbf{k}}-E^d_{\mathbf{k}}\right)^2+4|V|^2}\\&\equiv\sqrt{\left(E^-_\Gamma+\frac{\hbar^2k^2}{2m^*_-}\right)^2+4|V|^2}\end{aligned} \tag{A3}$$

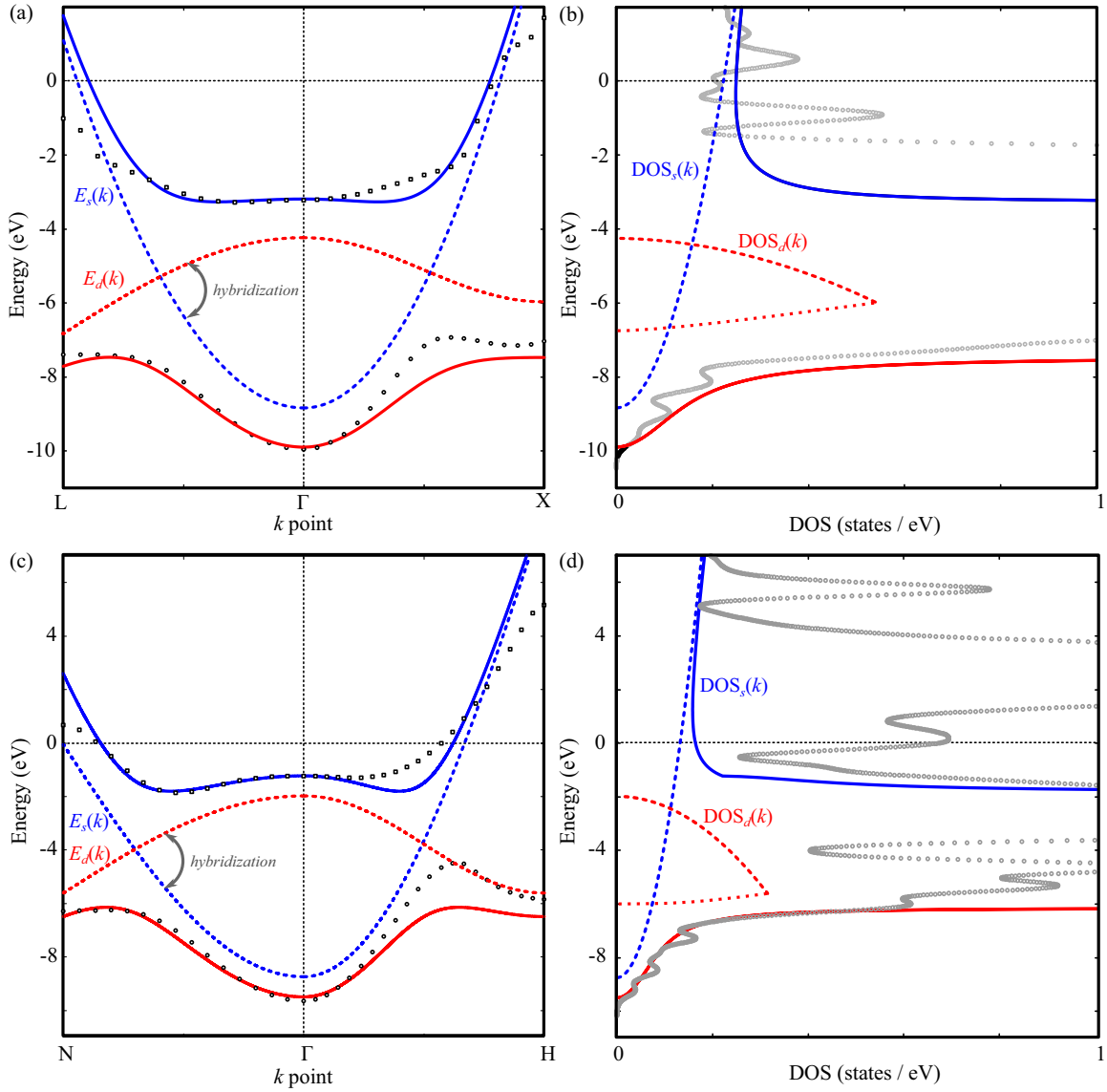

FIG. 4. Energy dispersion $E(k)$ and density of states (DOS) of Au and W. The energy dispersion and DOS of Au are shown in panels (a) and (b), respectively, while panels (c) and (d) show those of W. Data points were obtained using DFT. In panels (a) and (c), blue and red dotted lines indicate the energy dispersion of s and d electron without hybridization, respectively. The hybridized dispersion are illustrated with blue and red full lines. In panels (b) and (d), the dashed and full lines illustrate DOS without and with hybridization, respectively. While the energy dispersion only shows the hybridized band, the DOS shows the total DOS obtained using DFT. The orbital hybridization increases the DOS near the Fermi level.

can be used to obtain

$$E_\Gamma^- = E_0^s - E_0^d, \quad \frac{1}{m_-^*} = \frac{1}{m_s^*} - \frac{1}{m_d^*},$$

and hybridization energy V. The $E_0^{s'd}$ and effective masses can then be obtained from $E_\Gamma^\pm$ and $m_\pm^*$, respectively.

[1] J. Barnaś, A. Fert, M. Gmitra, I. Weymann, and V. K. Dugaev, From giant magnetoresistance to current-induced switching by spin transfer, Phys. Rev. B **72**, 024426 (2005).

[2] A. Brataas, Y. Tserkovnyak, G. E. W. Bauer, and P. J. Kelly, Spin pumping and spin transfer, in *Spin Current* (Oxford University Press, Oxford, 2018).

[3] J. Xiao, G. E. W. Bauer, and A. Brataas, Spin-transfer torque in magnetic tunnel junctions: Scattering theory, Phys. Rev. B **77**, 224419 (2008).

[4] A. B. Cahaya and M. A. Majidi, Effects of screened Coulomb interaction on spin transfer torque, Phys. Rev. B **103**, 094420 (2021).

[5] Y. Tserkovnyak, A. Brataas, and G. E. W. Bauer, Spin pumping and magnetization dynamics in metallic multilayers, Phys. Rev. B **66**, 224403 (2002).

[6] Y. Tserkovnyak, A. Brataas, and G. E. W. Bauer, Enhanced Gilbert Damping in Thin Ferromagnetic Films, Phys. Rev. Lett. **88**, 117601 (2002).

[7] A. B. Cahaya, Antiferromagnetic spin pumping via hyperfine interaction, Hyperfine Interact. **242**, 46 (2021).
[8] A. B. Cahaya, Adiabatic limit of Rkky range function in one dimension, J. Magn. Magn. Mater. **547**, 168874 (2022).
[9] K. Carva and I. Turek, Spin-mixing conductances of thin magnetic films from first principles, Phys. Rev. B **76**, 104409 (2007).
[10] E. Šimánek, Gilbert damping in ferromagnetic films due to adjacent normal-metal layers, Phys. Rev. B **68**, 224403 (2003).
[11] A. B. Cahaya, A. O. Leon, and G. E. W. Bauer, Crystal field effects on spin pumping, Phys. Rev. B **96**, 144434 (2017).
[12] M. Weiler, M. Althammer, M. Schreier, J. Lotze, M. Pernpeintner, S. Meyer, H. Huebl, R. Gross, A. Kamra, J. Xiao, Y.-T. Chen, H. J. Jiao, G. E. W. Bauer, and S. T. B. Goennenwein, Experimental Test of the Spin Mixing Interface Conductivity Concept, Phys. Rev. Lett. **111**, 176601 (2013).
[13] D. L. R. Santos, P. Venezuela, R. B. Muniz, and A. T. Costa, Spin pumping and interlayer exchange coupling through palladium, Phys. Rev. B **88**, 054423 (2013).
[14] L. Zhu, D. C. Ralph, and R. A. Buhrman, Effective Spin-Mixing Conductance of Heavy-Metal–Ferromagnet Interfaces, Phys. Rev. Lett. **123**, 057203 (2019).
[15] M. M. Sigalas and D. A. Papaconstantopoulos, Calculations of the total energy, electron-phonon interaction, and Stoner parameter for metals, Phys. Rev. B **50**, 7255 (1994).
[16] B. Zellermann, A. Paintner, and J. Voitländer, The Onsager reaction field concept applied to the temperature dependent magnetic susceptibility of the enhanced paramagnets Pd and Pt, J. Phys.: Condens. Matter **16**, 919 (2004).
[17] A. A. Povzner, A. G. Volkov, and A. N. Filanovich, Electronic structure and magnetic susceptibility of nearly magnetic metals (palladium and platinum), Phys. Solid State **52**, 2012 (2010).
[18] R. M. Sitorus, A. Azhar, A. B. Cahaya, A. R. T. Nugraha, and M. A. Majidi, Theoretical study of complex susceptibility of Pd and Pt, J. Phys.: Conf. Ser. **1816**, 012044 (2021).
[19] P. W. Anderson, Localized magnetic states in metals, Phys. Rev. **124**, 41 (1961).
[20] J. R. Schrieffer and P. A. Wolff, Relation between the Anderson and Kondo Hamiltonians, Phys. Rev. **149**, 491 (1966).
[21] J. B. Goodenough, Band structure of transition metals and their alloys, Phys. Rev. **120**, 67 (1960).
[22] S. J. Clark, M. D. Segall, C. J. Pickard, P. J. Hasnip, M. I. J. Probert, K. Refson, and M. C. Payne, First principles methods using castep, Z. Kristallogr.-Cryst. Mater. **220**, 567 (2005).
[23] P. Giannozzi, S. Baroni, N. Bonini, M. Calandra, R. Car, C. Cavazzoni, D. Ceresoli, G. L. Chiarotti, M. Cococcioni, I. Dabo, A. D. Corso, S. de Gironcoli, S. Fabris, G. Fratesi, R. Gebauer, U. Gerstmann, C. Gougoussis, A. Kokalj, M. Lazzeri, L. Martin-Samos *et al.*, QUANTUM ESPRESSO: A modular and open-source software project for quantum simulations of materials, J. Phys.: Condens. Matter **21**, 395502 (2009).
[24] G. Pizzi, V. Vitale, R. Arita, S. Blügel, F. Freimuth, G. Géranton, M. Gibertini, D. Gresch, C. Johnson, T. Koretsune, J. Ibañez-Azpiroz, H. Lee, J.-M. Lihm, D. Marchand, A. Marrazzo, Y. Mokrousov, J. I. Mustafa, Y. Nohara, Y. Nomura, L. Paulatto *et al.*, WANNIER90 as a community code: New features and applications, J. Phys.: Condens. Matter **32**, 165902 (2020).
[25] H. L. Wang, C. H. Du, Y. Pu, R. Adur, P. C. Hammel, and F. Y. Yang, Scaling of Spin Hall Angle in 3D, 4D, and 5D Metals from $Y_3Fe_5O_{12}$/Metal Spin Pumping, Phys. Rev. Lett. **112**, 197201 (2014).
[26] A. Jain, S. P. Ong, G. Hautier, W. Chen, W. D. Richards, S. Dacek, S. Cholia, D. Gunter, D. Skinner, G. Ceder, and K. A. Persson, Commentary: The Materials Project: A materials genome approach to accelerating materials innovation, APL Mater. **1**, 011002 (2013).
[27] D. Rodic, M. Mitric, R. Tellgren, H. Rundloef, and A. Kremenovic, True magnetic structure of the ferrimagnetic garnet $Y_3Fe_5O_{12}$ and magnetic moments of iron ions, J. Magn. Magn. Mater **191**, 137 (1999).
[28] X. Ma, G. Yu, C. Tang, X. Li, C. He, J. Shi, K. L. Wang, and X. Li, Interfacial Dzyaloshinskii-Moriya Interaction: Effect of 5*d* Band Filling and Correlation with Spin Mixing Conductance, Phys. Rev. Lett. **120**, 157204 (2018).
[29] E. Šimánek and B. Heinrich, Gilbert damping in magnetic multilayers, Phys. Rev. B **67**, 144418 (2003).
[30] K. Persson, Materials data on Co (SG:194) by Materials Project (2016), doi: 10.17188/1263614.